# We are IntechOpen,
# the world's leading publisher of
# Open Access books
# Built by scientists, for scientists

## 6,900
Open access books available

## 186,000
International authors and editors

## 200M
Downloads

## 154
Countries delivered to

Our authors are among the

## TOP 1%
most cited scientists

## 12.2%
Contributors from top 500 universities

BOOK CITATION INDEX
CLARIVATE ANALYTICS
INDEXED

**WEB OF SCIENCE**™

Selection of our books indexed in the Book Citation Index
in Web of Science™ Core Collection (BKCI)

# Interested in publishing with us?
# Contact book.department@intechopen.com

Numbers displayed above are based on latest data collected.
For more information visit www.intechopen.com

# Longitudinal Changes of Structural and Functional Connectivity and Correlations with Neurocognitive Metrics

*Yongxia Zhou*

## Abstract

Revealing brain functional and micro-structural changes over a relatively short period at individual levels are especially important given that many risks associated with age including vascular and neuroinflammation increases and could confound the baseline fMRI parametric images. Cellular-level axonal injury and/or demyelination as well as dispersed mesoscopic level substance abnormal aggregation and structural/functional abnormality could occur in short subacute/acute phases, while literatures related to longitudinal changes with age are limited with only our previous fMRI findings. Longitudinal data were used to characterize these multi-parameters including random intercept and interval per individual. No significant age by gender interactions have been found to either DTI fractional anisotropy (FA) or diffusivity metrics. The interval effective regions showed longitudinal change of FA and radial diffusivity (RD)/axial diffusivity (AX) values remained similar to the aging results found with cross-sectional data. Significant correlations between DTI and fMRI metrics as well as between imaging and neurocognitive data including speed and memory were found. Our results indicate significant and consistent age, gender and apolipoprotein E (APOE) genotypic effects on structural and functional connectivity at both short-interval and cross-sectional ranges, together with correlational neurocognitive functions.

**Keywords:** microstructure, function connectivity, DTI, longitudinal change, neurocognitive test, correlation, age, APOE gene

## 1. Introduction

Functional connectivity based on MRI (fcMRI) measures simultaneous and synchronous neuronal activities at various regions connected intrinsically in brain with functional MRI time courses. In our recent study, we reported lower functional connectivity in posterior cingulate and temporal regions with aging within the default mode network (DMN) [1]. We also found higher fcMRI in the dorso-attentional network (DAN) (including in the dorso-lateral prefrontal cortex) at age, which could be due to the negative connectivity with DMN. Furthermore longitudinal changes in fcMRI occurred in regions similar to those demonstrating cross-sectional effects of age, with only a few small brain areas showing significant age by interval

or gender by interval effects. The rate of fcMRI longitudinal change, however, was not influenced significantly by baseline age or gender, after adjusting for baseline age and gender modulation effects in majority of brain regions, suggesting moderate linear interval effects of fcMRI longitudinal changes in brain. Our results from this relatively large cohort suggest that fcMRI variability from various networks in different scales might be useful to monitor brain changes in normal aging and preclinical stages of Alzheimer's disease [1]. As for diffusion tensor imaging (DTI), we used both voxel-wise four DTI metrics and tract-specific ROI analysis to investigate myelin and axonal integrity differences with age, gender and APOE genotype with four DTI metrics at baseline [2–5]. One of the main findings was the decreased fractional anisotropy (FA) but increased radial diffusivity (RD) with age based on both voxel-wise and tract-specific analyses indicating both axonal degeneration and demyelination [6, 7]. Dramatic decreases of FA with age, especially in participants over 50 years old, accompanied by increased RD suggest that white matter (WM) integrity declines with age. In contrast, changes in axial diffusivity (AX) and mean diffusivity (MD) with age are in two-way: higher AX and MD in some tracts and cortical regions including bilateral thalamic radiation and cingulum bundles, as well as decreased AX and MD in some long-distance fasciculus [8–11].

Regarding DTI and fMRI correlations, significant gray matter (GM) and WM correspondences based on GM atrophy and WM fractional anisotropy (FA) reductions in several brain regions were found in multiple sclerosis (MS) patients including primary visual cortex/optic radiation as well as somatosensory cortex/superior longitudinal fasciculus at baseline [12]. However, with disease progresses, these associations might be deteriorated and are not maintained [13–15], although each imaging feature at baseline and longitudinal time points remain consistent and highly correlated [16, 17]. The degree of change (or rate of change) of each metric is dependent on the sensitivity during the disease course [18–20]. For instance, GM atrophy and functional coordination decrement were found at follow-up visit in MS patients, in contrast to the usual observation of significant FA reductions and WM lesions predominantly in corpus callosum, periventricular areas, occipital horns and cingulum areas at baseline in MS compared to controls [12]. In mild traumatic brain injury (MTBI), 1 year after injury, there was measurable global brain atrophy, larger than that in control subjects. The anterior cingulate WM bilaterally and the left cingulate gyrus isthmus WM, as well as the right precuneal GM, showed significant decreases in regional volume in patients with MTBI over the 1st year after injury [21]. However at baseline, after normalization to supratentorial brain volume, there were no significant regional brain volume differences between patients with MTBI at the time of their initial visit and the control group. Our observations complement these findings and indicate that specific brain structure such as the cingulum and precuneus may be more vulnerable to long-term structural changes [22, 23].

It had been reported that baseline imaging findings including micro-structure integrity measured with DTI can predict functional activation and coordination at follow-ups. We had reported that FA measure at baseline predicted follow-up functional coordination score from fMRI data (r = 0.68, P = 0.007), indicating a possible initial WM inflammatory factor to the subsequent neurodegenerative processes in MS patients [12]. We also found that baseline composite imaging metrics can predict cognitive function and neuropsychological scores. For instance, in MTBI, the clinical symptom at follow-up visit could be predicted with high accuracy from baseline imaging features with r = −0.82, P < 0.001 for depression; r = −0.65, P = 0.01 for anxiety; r = −0.71, P = 0.005 for fatigue; and r = −0.67, P = 0.008 for post-concussion syndrome (PCS) [23]. Revealing the brain micro-structural changes over a relatively short period at individual levels are especially important given that many risks associated with age including vascular and

neuroinflammation increases and could confound the baseline parametric images of each individual. However, literatures related to longitudinal changes of neuroimaging data with age are still limited [24].

The goals of this study were to assess baseline and longitudinal age and gender-related changes with neuroimaging and neurocognitive data from a large sample of healthy older adults, as well as apolipoprotein E (APOE) genotypic effects. The strengths of this study are the extensive and well-characterized large sample of older adults, and multiple imaging metrics including advanced fcMRI, four DTI (FA, MD, RD, AX) to capture extensive properties of functional connectivity and white matter myelination at both baseline and longitudinal follow-up time points. Both conventional whole brain voxel-wise analyses and fiber track-specific ROI quantification measures that are more robust and less prone to registration error were used to increase the white matter myelin detection specificity. Beside previous fcMRI findings [1], we also investigate longitudinal changes of multiple DTI and fMRI metrics as well as neurocognitive tests. The correlations among different imaging metrics as well as between neuroimaging findings and neurocognitive scores were quantified to better illustrate the full spectrum of multiple phenotypic data.

## 2. Methods

### 2.1 Participants

We studied 572 cognitively normal participants in the neuroimaging substudy from the Baltimore Longitudinal Study of Aging (BLSA) who had DTI assessments. Exclusion criteria were as follows: subjects with excessive motions and unwanted imaging qualities (N = 17 and 30 scans); subjects with incidental findings of brain lesions or other central nervous diseases, such as, Parkinson's disease (N = 4). Twenty individuals aged 24–39, 39 individuals aged 40–49, 51 aged 50–59, 137 aged 60–69, 186 aged 70–79, and 138 aged 80–89.

Three hundred and eighty-seven participants (68%) had available APOE genotype information, 107 APOE ε4+ and 280 APOE ε4− participants were further divided into six sub-groups based on the APOE isoforms. These sample characteristics are shown in **Table 1**. Two hundred and forty-five subjects had longitudinal follow-up (interval range 0.9–3.5 years, mean interval of 1.9 ± 0.6 years) and were used to characterize aging effects at short interval. Neurocognitive data from 21 cognitive tests with 59 variables that measure multiple cognitive functionalities including visual perception and attention, learning and memory encoding and recall, language fluency, and executive function for each participant was collected at the same day of the MRI scan [25]. After post-processing with normalization, 52 test scores were used for further analysis including correlation tests.

### 2.2 Imaging parameters

MRI imaging was obtained with a 3T whole-body scanner (Philips, Achieva) at National Institute of Aging, using an eight-channel head coil. The DTI sequence was evaluated previously and found to have good intra-site reliability and inter-section reproducibility [1]. Specifically, standard echo-planar imaging (EPI)-based DTI protocol was performed during the routine 45-min scan (TR/TE = 6801/75 msec, flip angle = 90°, FOV = 212 × 212 mm$^2$, spatial resolution = 0.83 × 0.83 × 2.2 mm$^3$, 65 slices to cover the whole cerebrum). Thirty-two diffusion gradient directions (diffusion gradient time Δ = 36.3 ms and pulse duration δ = 16 ms) with b-factor of 700 s/mm$^2$ and a total of 3:58 min for each run as well as two identical runs were obtained for each subject.

| Characteristic | All DTI baseline | ε4/ε4 | ε3/ε4 | ε2/ε4 | ε3/ε3 | ε2/ε3 | ε2/ε2 | Both DTI and fMRI |
|---|---|---|---|---|---|---|---|---|
| Total n | 572 | 4 | 95 | 8 | 219 | 59 | 2 | 236 |
| Age, years; mean ± SD | 69.7 ± 13.4 | 68.4 ± 16.8 | 67.0 ± 12.1 | 69.4 ± 12.6 | 70.1 ± 11.3 | 70.0 ± 10.1 | 75.9 ± 16.4 | 72.0 ± 12.2 |
| Gender n; women/men | 311/261 | 3/1 | 56/39 | 7/1 | 115/104 | 30/29 | 1/1 | 135/101 |
| Education, years; mean ± SD | 17.1 ± 2.7 | 17.5 ± 1.0 | 17.4 ± 2.5 | 17.1 ± 2.1 | 16.9 ± 2.6 | 17.6 ± 2.2 | 16.0 ± 2.8 | 17.0 ± 2.4 |
| MMSE at visit | 28.6 ± 1.5 | 28.3 ± 1.5 | 28.8 ± 1.4 | 29.5 ± 0.6 | 28.4 ± 1.6 | 28.5 ± 1.4 | 29.0 ± 1.4 | 28.8 ± 1.3 |

**Table 1.**
*Sample characteristics for the whole sample and six APOE genotypic sub-groups.*

A standard echo-planar imaging (EPI) resting-state (RS)-fMRI protocol (TR/TE = 2000/30 msec, flip angle = 75°, FOV = 240 × 240 mm$^2$, voxel size =3 × 3 × 4 mm$^3$, 37 slices) was performed during an approximately 45-min brain MRI protocol. A total of 180 volumes were acquired during the 6-min RS-fMRI scan. Participants were instructed to remain still, with eyes open and focused on a cross fixation, and encouraged to relax during the scan. A 3-dimensional T1-weighted MPRAGE (magnetization prepared rapid gradient-echo imaging) sequence (TR/TE/TI = 6.8/3.2/849.2 msec, FA = 8°, FOV = 192 × 256 × 256 mm$^3$, voxel size = 1.2 × 1 × 1 mm$^3$) was acquired in sagittal-view for segmentation of tissue types and registration/normalization of EPI images to MNI space.

## 2.3 Image processing

DTI data were first pre-processed with the diffusion toolkit toolbox (http://trackvis.org) to obtain the FA/RD/AX/RD values in original b0 space. For the FA/RA/AX/RD quantification, the FMRIB, Software Library (FSL, http://fsl.fmrib.ox.ac.uk/fsl) tract-based spatial statistics toolbox steps 1–2 (i.e., preprocessing, brain mask extraction with FA > 0.2 and normalization) were used for registration of all participants' FA into the FSL 1-mm white matter skeleton template. The transformation of the individual FA data to the FSL Montreal Neurological Institute (MNI) template with 1-mm isotropic voxel size, was implemented with the nonlinear registration tool FNIRT based on a b-spline representation of the registration warp field. After normalization of FA map to the MNI space, tract-specific mean FA values were obtained in 20 regions from the well-defined probabilistic tract template (FSL/JHU ICBM atlas). Quantitative MD/AX/RD values were obtained by applying the same transformation from individual FA to template space and computed with tract-specific values [1].

The anatomic T1-MPRAGE and 4D EPI functional data were preprocessed using both FSL and Analysis of Functional NeuroImages (AFNI) programs (adapted scripts from http://www.nitrc.org/projects/fcon_1000 developed based on FSL and AFNI). For structural MPRAGE data used for fMRI data normalization, preprocessing included reorientation to the right-posterior-inferior convention and skull stripping, and segmentation into three tissue types: GM, WM, and cerebrospinal fluid (CSF). The segmental tissue masks were used to derive the nuisance fMRI signals in WM and CSF. Finally, the MPRAGE image was co-registered with the fMRI data and normalized to the Montreal Neurologic Institute (MNI) 152-brain template with 2-mm isotropic voxel size [1, 12].

For fcMRI processing, the first four volumes of the RS-fMRI data of each subject were discarded for scanner and image stability. Preprocessing steps for RS-fMRI data included rigid alignment of the time frames using AFNI motion correction algorithms, spatial smoothing using a Gaussian kernel with 6 mm full-width-at-half-maximum (FWHM), and band-pass temporal filtering of 0.005–0.1 Hz to improve signal-to-noise ratio. Removal of nuisance signals was then performed using a Gaussian regression model after co-registration to MPRAGE data. Namely, motion parameters, global signal, and signals derived from CSF and WM based on the tissue masks were modeled in the Gaussian linear mixed model, and residual signal at each voxel was maintained for further analyses. Finally the residual 4D fMRI data after regression were transformed to MNI standard space [26]. A DMN seed including both medial prefrontal cortex (MED) (MNI center: 0, 48, 23 mm) and posterior cingulate cortex (PCC) (MNI center: 26, 248, 39 mm) with a combined volume of 4112 mm$^3$ (each seed of 2056 mm$^3$) was used. We refer to this seed as the combined core seed. We chose the combined core seed over separate PCC and MED seeds because the latter approach generates different and incomplete DMN

connectivity patterns [27], whereas the combined core seed yields consistent and complete depictions of DMN [26]. Whole brain voxel-wise Pearson correlation coefficients were computed between the average time series within the seed and the time course of each fMRI voxel in the brain. Finally Z-statistics were derived voxel-wise. 2nd-level Gaussian random field (GRF) and family-wise corrections were applied to derive the functional connectivity (FC) map with FSL toolbox.

In addition to the combined core seed, the fcMRI generated from other seeds were also evaluated to study the systematic-level fcMRI, with a total of 26 seeds [1]. The other 25 seeds included 12 conventional regions of different sub-areas of DMN (e.g., PCC and intra-parietal sulcus), three thalamic (left, right, and whole thalamus) and seven subthalamic seeds [28], and three subcortical seeds (caudate and putamen from the MNI template, and hypothalamus from an in-house developed probability map) [29]. The conventional 12 seeds were derived from the script seed library (http://www.nitrc.org/projects/fcon_1000), including the hippocampal formation and frontal eye field (FEF) seeds that generated the task-positive networks (i.e., these networks are more active at task-conditions, in contrast to resting state). All seeds were well-evaluated and validated previously [27, 28, 30]. The global mean Z-values were obtained from the fcMRI maps generated from each of 26 seeds to study age and gender effects as well, by averaging the fcMRI Z-maps over the whole brain with a threshold of GRF cluster-corrected $P < 0.01$.

Meanwhile in the resting state, fractional amplitude of low-frequency fluctuations (fALFF) has been shown to be higher in the DMN regions that are active and it had also been reported that task-related (e.g., working memory, motor visual stimuli and cognitive tasks) alterations of low-frequency oscillations could reflect real-time neuronal activity [28]. The idea of fALFF method was to scale the summary of amplitude at low-frequency band (e.g., 0.01–0.08 Hz) to the summary of amplitude across whole band to remove white and physiological noise. In this study, the resting-state fALFF Z-value at baseline and longitudinal changes of fALFF, as well as correlations with the age and other fcMRI/DTI neuroimaging metrics were performed from 236 participants with available data resource.

## 2.4 Statistical analyses

For DTI, effects of age, gender and APOE genotype were studied at both whole-brain voxel-wise level and tract-specific ROI analyses using the four DTI metrics-FA, RD, AX and MD. Linear mixed effects (LME) model was applied to characterize both baseline and longitudinal effects of age, gender and age by gender interactions of the four metrics [1, 31]. We used the MATLAB Statistics toolbox (www.mathworks.com, R2015b) and in-house programs to perform model fitting as listed in Eq. (1). Longitudinal data were incorporated to characterize the longitudinal change of DTI metrics with interval as the prediction parameter as well. In order to account for within-individual correlations stemming from follow-up data, we included random intercept and random interval (i.e., random slope) terms per individual in LME.

$$\begin{aligned} DTI \sim \beta_0 &+ \beta_1 \text{ gender} + \beta_2 \text{ baseage} + \beta_3 \text{ interval} \\ &+ \beta_4 \text{ interval:baseage} + \beta_5 \text{ gender:baseage} + \beta_6 \text{ interval:gender} \end{aligned} \quad (1)$$

For whole-brain analyses, voxel-wise linear regression with DTI metrics as the dependent variable and age as an independent variable using SPM12 software (Statistical Parametric Mapping, http://fil.ion.ucl.ac.uk/spm/software/spm12) was implemented. Gender term was included as a covariate. Then two-sample t-test comparison using baseline DTI data was also implemented to study gender differences between women and men, and age was used as a covariate [32].

For tract-specific ROI-based analyses, the mean value of each regional FA and diffusivity (i.e., RD, AX and MD) analysis were quantified with FSL toolbox and in-house programs developed with MATLAB (www.mathematics.com). Both linear and quadratic fitting were used to examine white matter myelination along aging trajectories. Mean values of all six APOE genotypes were derived from each ROI to form the waveform and multiple-group comparisons of the four DTI metrics stratified by genotypic isoforms were performed in MATLAB toolbox.

To characterize cross-sectional and longitudinal changes in fcMRI, we used a LME model, similar to DTI longitudinal data model with the same analyses algorithm as listed in Eq. (2). In order to account for cross-sectional differences across individuals, we included baseline age and gender as covariates. Baseline age was centered at group mean of 69.4 years. Men were coded as 0.5 and women as −0.5. Time interval in years between baseline and follow-up was included to capture longitudinal change in fcMRI. We also included interaction terms with interval, random intercept and interval terms to compute longitudinal rates of fcMRI change accounting for baseline age and gender interactions [1].

$$fcMRI \sim \beta 0 + \beta 1\ baseage + \beta 2\ gender + \beta 3\ interval$$
$$+ \beta 4\ interval{:}baseage + \beta 5\ gender{:}baseage + \beta 6\ interval{:}gender \quad (2)$$

Conventional statistical comparison (with relatively smaller number of participants) using a two-sample t-test at baseline and 3 years follow-ups, adjusting for gender, with the same statistical threshold as used in LME model (P < 0.01 and cluster size ≥10 voxels) was used for longitudinal fALFF data quantification. To validate the age and gender effects observed in LME model, SPM-based conventional regression model including general linear correlational analysis between age and fcMRI adjusted for gender, and comparison between women and men group adjusted for age were performed as well.

## 3. Results

### 3.1 Age effects on DTI

Whole brain DTI FA showed prominent aging effects (i.e., reduced FA with aging) in the main projections fibers including cingulum bundle and superior longitudinal fasciculus (P < 0.00001) (**Figure 1a**). The monotonically reduction of FA was observed in relatively older subject with age larger than 50 years old that construe the majority of the sample size. RD, on the other hand, showed only significantly higher RD values with age in bilateral thalamic radiations, bilateral somatosensory cortex, visual cortex, anterior and posterior cingulate gyri, middle temporal cortex including hippocampus, subcallosal cortex and posterior cerebellum (P < 0.01, cluster size = 10). Very small clusters and primarily in the cerebellum was found to have lower RD along the age (**Figure 1b**). Axial diffusivity showed significantly higher AX values with age in some similar regions to RD including bilateral thalamic radiations, bilateral somatosensory cortex, visual cortex, posterior cerebellum and superior corona radiata tract (P < 0.01, cluster size = 10). In contrast to RD and FA, AX was also significantly lower in white matter regions including bilateral cortico-spinal tract, inferior longitudinal fasciculus, optic radiation and cerebellum (**Figure 1c**). MD shows almost a similar aging pattern as of AX (**Figure 1d**) [1].

As expected, all the tract-based ROI showed significant aging effects (i.e., reduced FA with age) after adjustment for multiple comparisons (r = 0.3–0.7, mean r = 0.5, corrected P < 0.0001). Quadratic fitting of FA from 20 track-specific ROIs showed
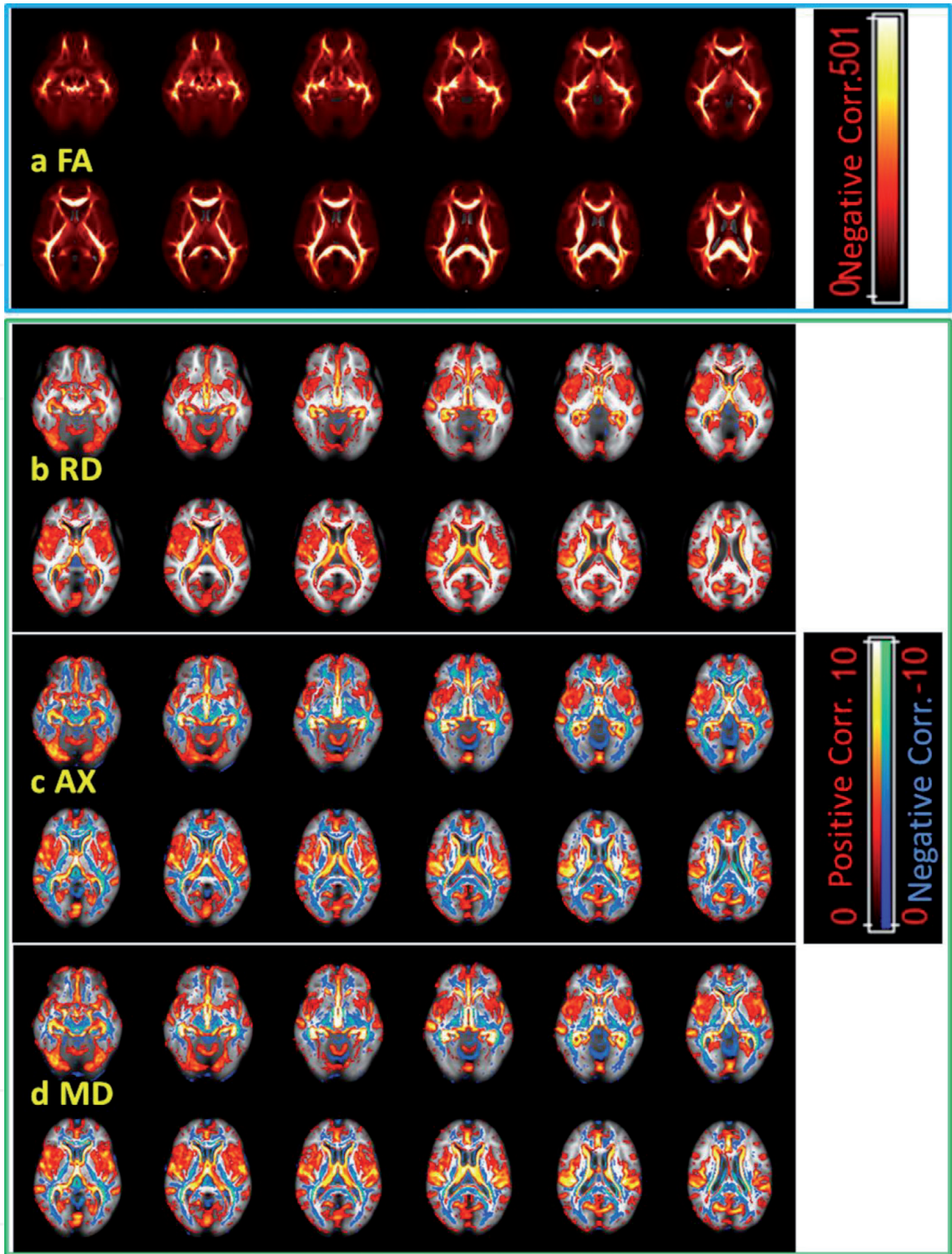
**Figure 1.**
*(a) Prominent aging effects were demonstrated with negative correlation between voxel-wise FA and age, i.e., decreased FA along the age (statistical T map, P < 0.01, cluster size = 10) for all brain regions. On the other hand, RD was increased along the age for some of the brain regions including somatosensory cortex and cingulum bundle (b). There are both increases and decreases of AX (c) and MD (d) in different brain regions along the age, and the changes of AX and MD have very similar patterns (all P < 0.01, cluster size = 10). Background image was derived from average of all subjects' FA maps in MNI space.*

aging trajectories with maturation age (i.e., mean FA reaches maximum) falling between [24, 28–41] years. The relatively earlier maturation age was found in the major forceps and bilateral thalamic radiation (28–33 years) and later maturation age from bilateral hippocampal portion of the cingulum and corticospinal tracts (39–42 years) (**Figure 2**). The tract-based ROI that has the earliest maturation age with highest FA at 27.9 years is the major forceps. The left hippocampal portion of the cingulum bundle
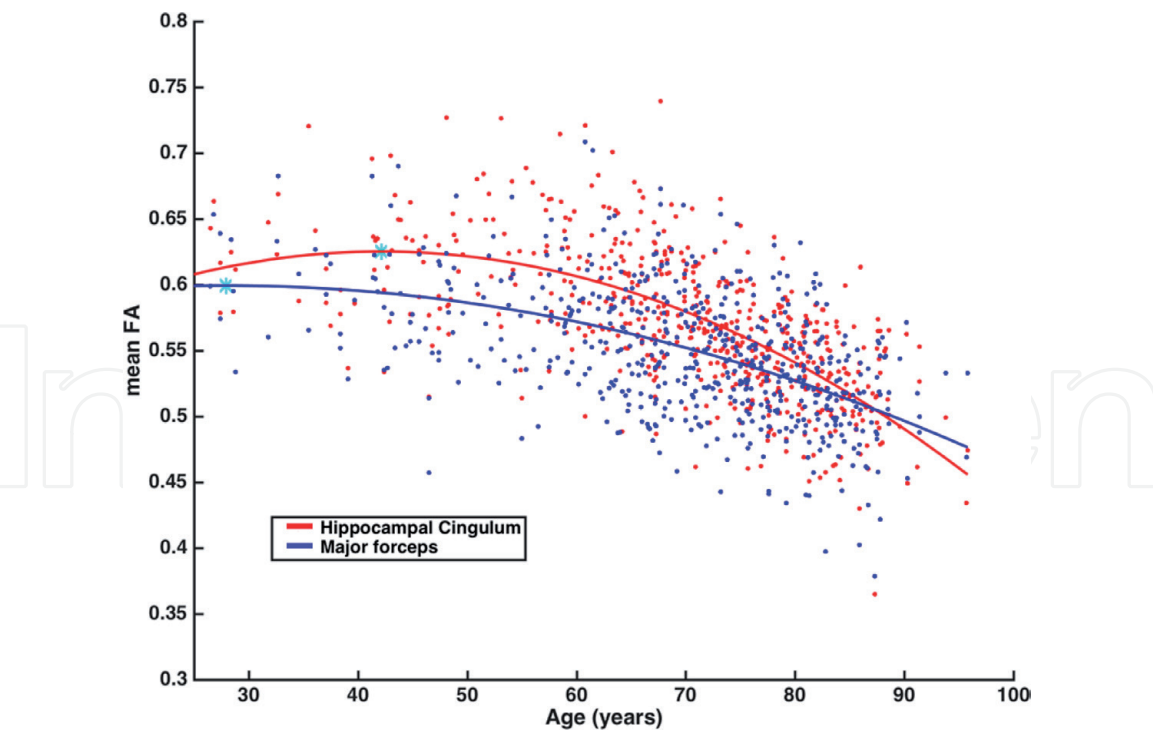
**Figure 2.**
*Quadratic aging trajectories of two tract-specific ROIs. Star (cyan color) indicates maturation age when mean FA of the tract each tract-specific ROI reaches maximum. Major forceps has the earliest maturation age, with highest FA at 27.9 years (blue color). While the left hippocampal portion of the cingulum bundle has the latest maturation age, with highest FA at 42.1 years (red color).*

has the latest maturation age (42.1 years). While the diffusivity measures from tract-based ROIs showed mostly linearly increases of diffusivity along the age with RD, and some tracts showed no significant aging effects based on AX or MD [1].

Using diffusion toolkit (http://www.nitre.org/projects/trackvis/) with an advanced tensorline propagation algorithm for fiber tracking, we found tracts that play important roles in memory and cognitive function also illustrated significant aging effects, including fiber tract numbers of the fornix that connects the hippo-campus to the whole brain, and fibro bundles connecting bilateral parahippocam-pus to the whole brain were decreased significantly with aging (both $P < 0.00001$).

### 3.2 Longitudinal change of FA

Based on LME model, no significant age by gender interactions have been found to either FA or diffusivity metrics in the whole-brain voxel-wise analyses indicating aging and gender effects can be studied independently (**Figure 3a**). The interval effective regions estimated from LME model showed longitudinal change of FA and RD/AX values remained similar to the aging results found with cross-sectional data as in **Figure 1** and gender effective brain regions ($P < 0.01$, cluster size = 10) (**Figure 3b**).

### 3.3 Gender effects on DTI

We found men had significantly higher FA in the hippocampal portion of the cingulum bundle, secondary somatosensory cortex, thalamus, cingulate and cerebellar regions compared to women, based on voxel-wise FA comparisons ($P < 0.01$). Lower FA in men than women in bilateral inferior longitudinal fasciculus, anterior thalamic radiation, frontal cortex and temporal part of the superior longitudinal fasciculus were also observed ($P < 0.01$, cluster size = 10). Scattered cortical regions including superior frontal, cerebellum and insular showed higher RD in men than women, and lower RD
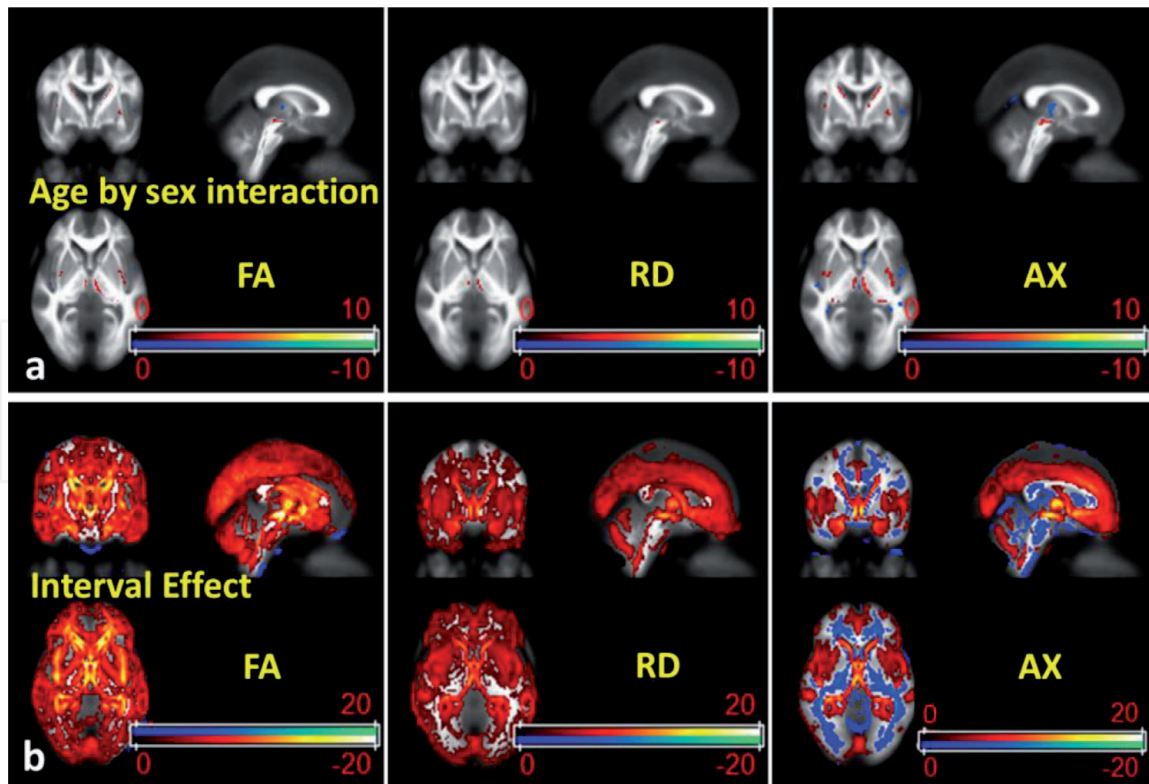
**Figure 3.**
*(a) Based on LME model, no significant age by gender interaction of DTI FA and diffusivity values across whole-brain with only a few outliers (P < 0.01). (b) The interval effect estimated from LME model using longitudinal data showed longitudinal change of FA, RD and AX values (MD is almost the same as AX) in brain regions similar to the baseline aging effects (1–3 years of interval of follow-up time; P < 0.01, cluster size = 10), suggesting an observable longitudinal change within a short time interval.*

in men only with small clusters in cerebellum. Furthermore AX and MD values in most of brain regions were higher in men than women (P < 0.01, cluster size = 10).
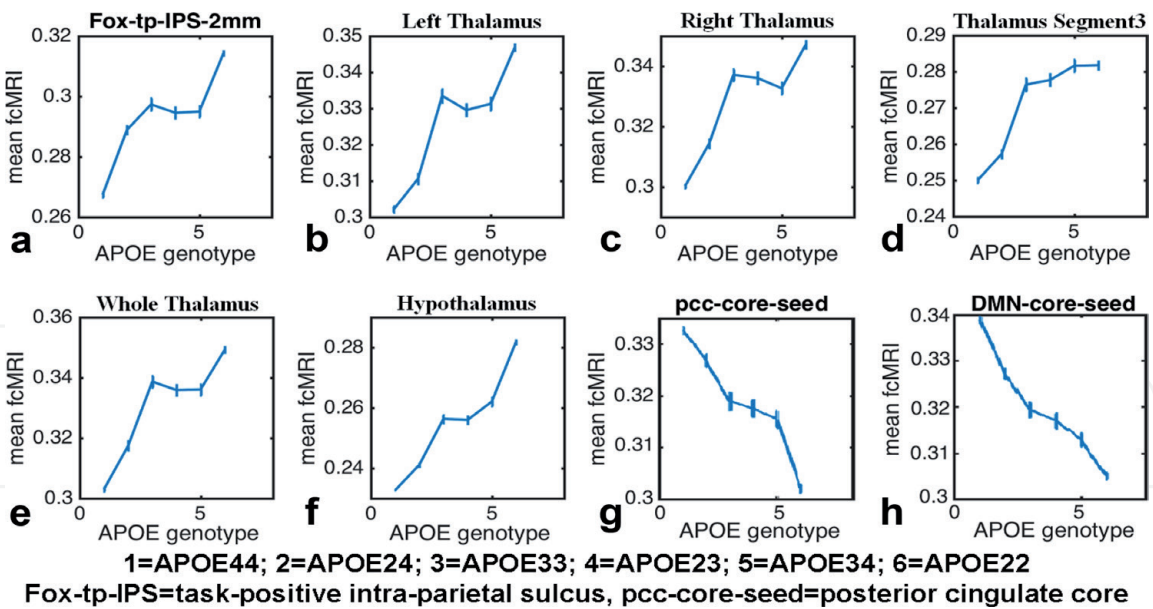
### 3.4 APOE genotype effects

Voxel-wise FA and MD comparisons between different APOE genotypes showed differences in scattered brain clusters (P < 0.01, cluster size = 10). Scattered brain regions showed both higher FA and higher diffusivity in APOE ε2/ε3 compared to APOE ε3/ε3, as well as comparing APOE ε3/ε4 to APOE ε3/ε3. Only RD was decreased in small clusters in APOE ε3/ε4 compared to APOE ε3/ε3 (P < 0.01, cluster size = 10). And AX comparison between APOE ε2/ε3 vs. APOE ε3/ε3 showed more brain regions with higher AX in APOE ε2/ε3 carriers. MD showed similar pattern as of AX.
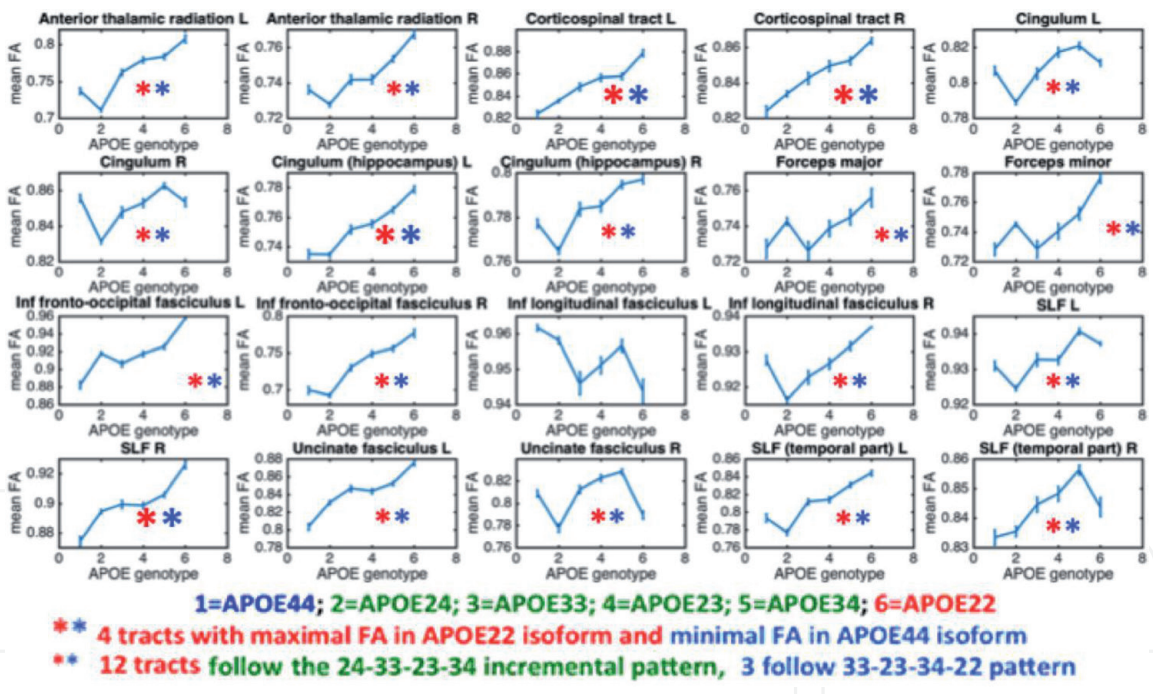
Furthermore, track-based mean FA stratified by different APOE genotype in majority of fibers demonstrated an incremental consistent pattern (44-24-33-23-34-22 chain, lowest in APOE44 and highest in APOE22 carriers); especially in right cortico-spinal tract and bilateral uncinate fasciculus (**Figure 4**). RD waveforms of 20 ROIs stratified by APOE genotype showed different waveforms than FA, with highest RD in APOE ε2/ε3 isoforms, and lower in APOE ε4+ carriers in all 20 ROIs. Both MD and AX measures showed very similar waveforms as of RD in 20 ROIs.

In addition, 11 out of 26 seed-based fcMRI strength (mean Z-value, with P < 0.001) stratified by different APOE genotype follow an incremental pattern with the 44-24-33-23-34-22 isoform including mean fcMRI seeding from subcortical thalamus (b–e), hypothalamus (f), and task-positive intra-parietal sulcus (a) as well as ventral medial prefrontal cortex; especially the hypothalamus (f) and from the thalamus segment 3 (d) that projected to visual cortex. On the other hand,

1=APOE44; 2=APOE24; 3=APOE33; 4=APOE23; 5=APOE34; 6=APOE22
Fox-tp-IPS=task-positive intra-parietal sulcus, pcc-core-seed=posterior cingulate core

**Figure 4.**
*Effects of APOE genotype on global fcMRI strength of task-positive networks seeding from intra-parietal sulcus (a), thalamus (b,c,d,e) and hypothalamus (f) demonstrated increasing patterns of fcMRI along with the 44-24-33-23-34-22 genotype. On the other hand, decreasing genotypic patterns of resting-state default mode networks (DMN) seeding from the posterior cingulum (g) and core seeds of DMN (h) were observed.*



1=APOE44; 2=APOE24; 3=APOE33; 4=APOE23; 5=APOE34; 6=APOE22
** 4 tracts with maximal FA in APOE22 isoform and minimal FA in APOE44 isoform
** 12 tracts follow the 24-33-23-34 incremental pattern, 3 follow 33-23-34-22 pattern
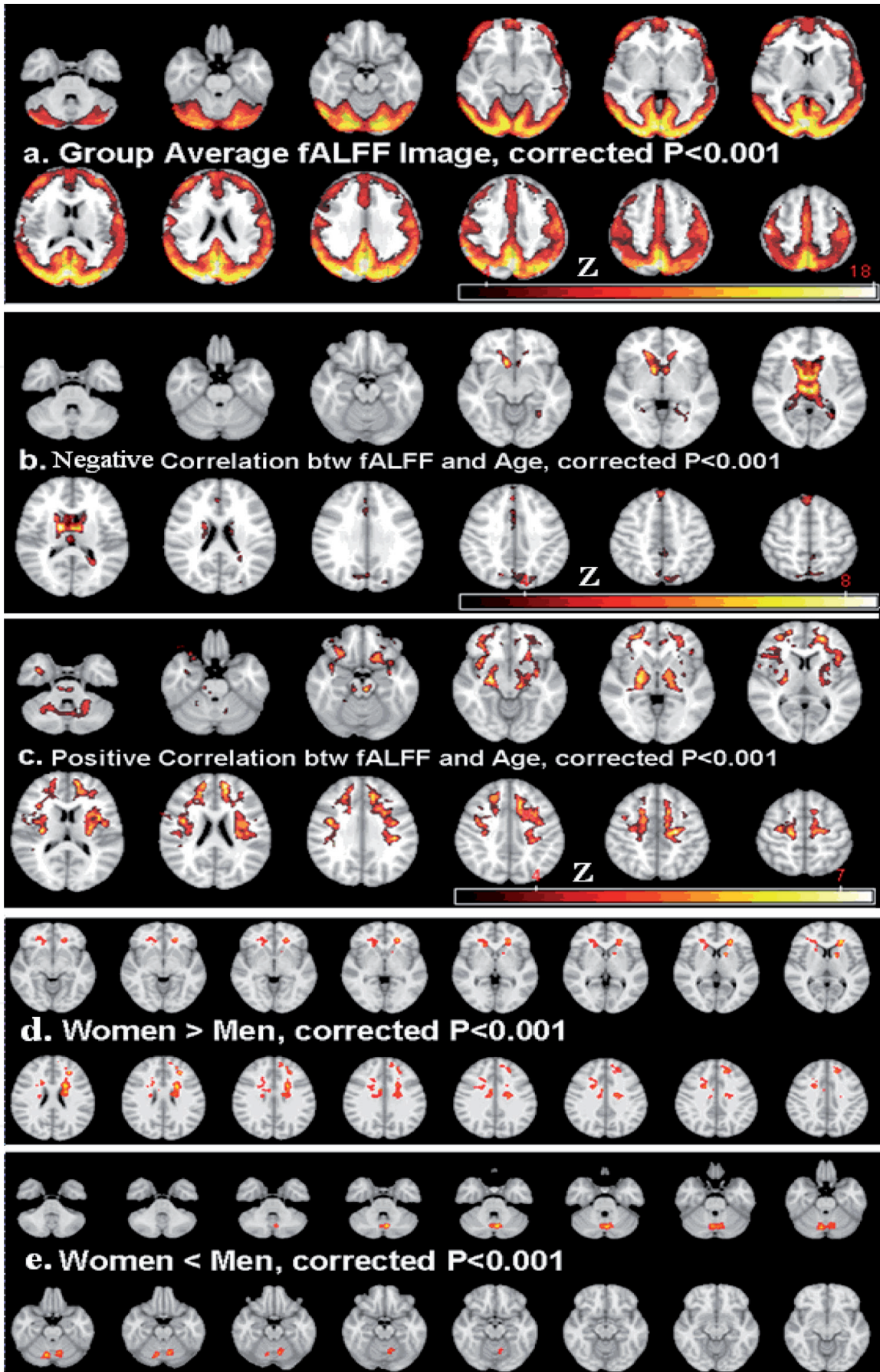
**Figure 5.**
*APOE genotypic effects on tract-specific DTI mean FA in 20 brain tracts. The mean FA of bilateral corticospinal, left cingulum and right superior longitudinal fasciculus tracts (marked with large **) follow the APOE 44-24-33-23-34 incremental pattern consistently. Inf = inferior; SLF = superior longitudinal fasciculus; L = left; R = right.*

gradual decrement of fcMRI strength with the APOE 44-24-33-23-34-22 genotypic chain of the DMN connecting from the posterior cingulate cortex (PCC) seed (g) and DMN core seed (h) had been observed as well (**Figure 5**).

### 3.5 fALFF and fcMRI results

As of fALFF, group mean image demonstrated higher fALFF in cortical gray matter with only temporal cortex largely spared (**Figure 6a**). Baseline aging effects

**Figure 6.**
*Functional activity measured with fALFF with group mean (a) (corrected P < 0.001) showing higher fALFF in cortical gray matter with only temporal cortex largely spared. Decreased activity with age in the superior middle frontal and precuneus as well as in the cortical caudate region (b), but increased activity in the cerebellum and bilateral frontal white matter (c) (both cluster corrected P < 0.001) were observed. Women group had higher fALFF Z values in frontal white matter area and small regions in caudate (d), while men group had higher fALFF in cerebellum (e) (both corrected P < 0.001).*

demonstrated decreased activity with age in the caudate, superior middle frontal and precuneus regions, but increased activity in the cerebellum and bilateral frontal white matter (P < 0.001) (**Figure 6b** and **c**). Average fALFF activity strength over the whole brain demonstrated magnificent aging effects (r = −0.28, P = 0.00001). Gender comparison showed slight difference with men had lower fALFF than women in small regions of caudate and frontal white matter clusters, but higher activity of men than women in the cerebellum (P < 0.001) (**Figure 6d** and **e**). Longitudinal comparison of baseline fALFF and 3 years later showed decreased functional activity in the right inferior parietal lobe and right occipital cortex; accompanied by increased activity in the front eye field region, left superior frontal and left temporal cortices (P < 0.01).

### 3.6 Correlations

LME model performed to available 52 neurocognitive tests at baseline also found significant aging effects (P < 0.00001) in almost all tests with worsening cognitive function at age. And similar longitudinal interval effects were found with a smaller significance level for each cognitive test (most P < 0.001).

Significant correlations between average Z-value of fcMRI strength in the DMN and neurocognitive tests were found as following: (1) between DMN Z and digital span test (DST) total score (r = 0.19, P < 0.00001); (2) between average DMN Z and Pegboard dominant (Dom) motor function score (r = 0.22, P < 0.00001); (3) between average DMN Z and Pegboard non-dominant (NonDom) mean score (r = 0.17, P = 0.00002); and (4) between average DMN Z and category fluency (FluenCat) test mean score (r = 0.12, P = 0.003). Interestingly, significant correlations between average DMN Z and graph-theory based resting-state functional network small-worldness properties were found as well, including: (1) between DMN Z and relative local efficiency (r = 0.15, P = 0.0002); (2) between DMN Z and absolute local efficiency (r = 0.17, P = 0.00002); (3) between DMN Z and relative global efficiency (r = 0.09, P = 0.02); (4) between DMN Z and absolute global efficiency (r = 0.1, P = 0.01); and (5) between DMN Z and small-worldness configuration (r = 0.15, P = 0.0001). Significant correlations between age and average DMN Z (r = −0.20, P < 0.00001; N = 608) are noted additionally.

Significant correlations between four DTI metrics (FA/MD/AX/MD) and neurocognitive functions were found including California verbal learning test (CVLT), Fluencat, Benton visual retention total errors (BVTOT), Dom and NDom tests that measure visual perception and memory dysfunction, language fluency, communication and social function, speed and accuracy, cognitive flexibility, visual attention, spatial orientation, working memory and executive function, as well as movement speed and motor function domains (most P < 0.0001). And correlations were found in all 20 tracts that connect to the whole brain indicating regional and global-wise associations between brain structure connectivity and neurocognitive alterations.

Significant correlations among imaging metrics were found as well including: (1) average whole-brain fALFF (a biomarker for functional activity) Z-value based on resting-state fMRI data and age (r = −0.28, P = 0.00002); (2) average fALFF Z and mean FA of whole brain (r = 0.26, P = 0.00007); (3) average DMN Z and mean FA of whole brain (r = 0.18, P = 0.007); and (4) average DMN Z and mean FA of DMN regions (r = 0.19, P = 0.004).

## 4. Discussion and conclusion

One of the main findings of DTI was the decreased FA but increased RD along the age based on both voxel-wise and track-specific analyses at both baseline and

longitudinal follow-up visits. Longitudinal data revealed similar rate of change of DTI metrics associated with age and gender as to cross-sectional results, indicating these changes were observable over a very short period (e.g., longitudinal interval of 1–3 years). Especially the significant decreases of FA along the age in most of brain regions suggest that white matter integrity reduces with age. Radial diffusivity (RD) increased with age in the regions that play important roles in memory, visual and motor function such as bilateral thalamic radiations, bilateral somatosensory cortex, visual cortex, anterior and posterior cingulate gyri, middle temporal cortex and hippocampus ($P < 0.01$, cluster size = 10). This suggested that demyelination process that resulted in radial space increases occurred in these brain tracts with age, and was also confirmed with significant reduced fiber-bundles from fornix and parahippocampus, as well as the latest maturation age of the cingulum bundle that was more vulnerable to demyelination and retrograde degeneration [1]. While changes in AX and MD are in two-way: increased AX and MD in some tracts and cortical regions including bilateral thalamic radiation and cingulum bundles, together with decreased AX and MD in some long-distance fasciculus including bilateral corticospinal tract, inferior longitudinal fasciculus and optic radiation. Lower FA and higher RD indicating axonal degeneration have been found in a small sample with similar age range [24, 33]. A few long commissure and association fibers including corpus callosum, cortico-spinal tract, cingulum bundle and superior longitudinal fibers might also undergo Wallerian degeneration [34] with increased RD but decreased AX along the age [1].

Consistent with the current view of neuroplasticity, neuroprotective and compensation roles of fMRI connectivity and activation [35–37], mean fcMRI values from DMN core and PCC core were lowest in the least risky APOE22 isoform, but highest in the most risky APOE44 isoform. And the waveforms of global DMN fcMRI strength decreases from the most to least risky genetic isoforms. However, for the subcortical regions including thalamus and hypothalamus seeds, the fcMRI increases from the expected most risky to least risky genetic isoforms. These changes of divergent waveforms of fcMRI from DMN and subcortical regions had also confirmed the opposite directions of resting-state DMN network and task-positive or attentional-recruitment networks, and might indicate less efficient or over-recruitment of neuronal source usage at most risky APOE44 carriers [38–41]. On the other hand, the DTI metric of FA from majority of fibers demonstrated an incremental consistent pattern from APOE44 to APOE22 carriers, indicating micro-structural integrity was associated positively and tightly with the genotypic functional role of each APOE allele.

Our results of significant imaging quantifications and neurocognitive tests indicate neuronal degeneration, functional disconnectivity as well as white matter deterioration (demyelination, Wallerian degeneration and structural connectivity) at age go parallel with each other, and present together with neurocognitive dysfunction (especially in the domains of memory, cognitive flexibility, visual perception and attention, and executive function). Similar correlation results were found between each tract-specific DTI metric and one-domain neurocognitive test suggest that regional correlations agree with each other, and significant structural connectivity-neurocognitive function correlations remain consistent across the whole brain. Associations between DMN functional connectivity and neurocognitive scores of memory, motor coordination and language social function are expected given the importance of DMN in these domains [42–44]. DMN also represents more global integration function based on the significant correlations between DMN fcMRI and local/global efficiencies of network analysis [45, 46]. Significant correlations were also found between global FA and global functional activity from fALFF; as well as between DMN fcMRI and DMN FA. Scattered longitudinal changes

and gender differences of fALFF were found with different patterns from fcMRI (largely decreased DMN but increased DAN regions of fcMRI). However, the spatial distribution pattern of fALFF was mainly in cortical gray matter (significantly higher in occipital, parietal and frontal cortices but with relatively lower activation pattern in temporal cortex). Although fALFF is not a good biomarker due to lack of functional and spatial specialization, it might be used in epoch-related task fMRI study to reflect neuronal activation under task conditions [28].

While our results are consistent with several published articles and are also in agreement with functional and structural connectivity findings [36, 47–50], current study is still limited to the scope of conventional fMRI and DTI sequence with normal aging samples. Further improvement of the technique with acceleration-based fMRI acquisition and multi-shell and multi-b-value DTI [32] as well as validation of our observations using other molecular imaging findings such as amyloid and tau imaging that provide pathological evidence besides the current neuroimaging findings are expected [23, 32, 51, 52]. It had been reported that task-based fMRI data could reflect specific cognitive function such as executive function, high-level cognitive function and communication skill, we expect more correlations could be found between fMRI data and neurocognitive scores in other cognitive domains [53, 54].

In conclusion, different sensitivities of DTI metrics in various brain regions have been observed of the age, gender and genotypic effects. For instance, FA measures showed age effects on white matter integrity across adulthood, with increases in FA through the 30's and 40's and subsequent decreases in middle-age and older adults. Accompanying the decreases of FA along the age in most of brain regions are the radial diffusivity increases that indicates demyelination process with age. AX and MD showed both lower and higher with age in different brain regions, suggesting possible axonal and Wallerian degenerations in these brain regions. We found longitudinal changes in both DTI and fcMRI in regions were similar to those demonstrating cross-sectional effects of age; for instance decreased fcMRI in DMN but increased fcMRI in anti-correlated DAN networks. The APOE genotypic signatures of FA and functional connectivity suggested possible tight associations between myelin/neuronal activation and APOE gene, indicating different roles of APOE alleles on brain structural conductivity, demyelination and neuroplasticity. Taken together, our neuroimaging and correlational neurocognitive results indicate significant and consistent age, gender and APOE genotypic effects on structural and functional connectivity at both baseline and longitudinal short-interval ranges.

**Author details**

Yongxia Zhou[1,2]

1 Department of Radiology, Columbia University, New York, NY, USA

2 Department of Biomedical Engineering, University of Southern California, Los Angeles, CA, USA

*Address all correspondence to: yongxia.zhou@yahoo.com

**IntechOpen**

# References

[1] Zhou Y. Functional Neuroimaging with Multiple Modalities. New York, USA: Nova Publishers; 2016

[2] Huster D, Yao X, Hong M. Membrane protein topology probed by (1) H spin diffusion from lipids using solid-state NMR spectroscopy. Journal of the American Chemical Society. 2002;**124**:874-883

[3] Basser PJ. Inferring microstructural features and the physiological state of tissues from diffusion-weighted images. NMR in Biomedicine. 1995;**8**:333-344

[4] Zhou XJ. Diffusion tensor imaging: Techniques and clinical applications. In: Conference Proceedings: Annual International Conference of the IEEE Engineering in Medicine and Biology Society IEEE Engineering in Medicine and Biology Society Annual Conference. Vol. 7. 2004. pp. 5223-5225

[5] Thiessen JD, Zhang Y, Zhang H, et al. Quantitative MRI and ultrastructural examination of the cuprizone mouse model of demyelination. NMR in Biomedicine. 2013;**26**:1562-1581

[6] Billiet T, Vandenbulcke M, Madler B, et al. Age-related microstructural differences quantified using myelin water imaging and advanced diffusion MRI. Neurobiology of Aging. 2015;**36**:2107-2121

[7] Gazes Y, Bowman FD, Razlighi QR, O'Shea D, Stern Y, Habeck C. White matter tract covariance patterns predict age-declining cognitive abilities. NeuroImage. 2016;**125**:53-60

[8] Sasson E, Doniger GM, Pasternak O, Tarrasch R, Assaf Y. Structural correlates of cognitive domains in normal aging with diffusion tensor imaging. Brain Structure and Function. 2012;**217**:503-515

[9] Agosta F, Dalla Libera D, Spinelli EG, et al. Myeloid microvesicles in cerebrospinal fluid are associated with myelin damage and neuronal loss in mild cognitive impairment and Alzheimer disease. Annals of Neurology. 2014;**76**:813-825

[10] Kochunov P, Glahn DC, Lancaster J, et al. Fractional anisotropy of cerebral white matter and thickness of cortical gray matter across the lifespan. NeuroImage. 2011;**58**:41-49

[11] Horch RA, Gore JC, Does MD. Origins of the ultrashort-T2 1H NMR signals in myelinated nerve: A direct measure of myelin content? Magnetic Resonance in Medicine. 2011;**66**:24-31

[12] Zhou Y. Neuroimaging in Multiple Sclerosis. New York, USA: Nova Publishers; 2017

[13] Bendfeldt K, Kuster P, Traud S, Egger H, Winklhofer S, Mueller-Lenke N, et al. Association of regional gray matter volume loss and progression of white matter lesions in multiple sclerosis—A longitudinal voxel-based morphometry study. NeuroImage. 2009;**45**:60-67

[14] Bjartmar C, Wujek JR, Trapp BD. Axonal loss in the pathology of MS: Consequences for understanding the progressive phase of the disease. Journal of the Neurological Sciences. 2003;**206**:165-171

[15] Bodini B, Khaleeli Z, Cercignani M, Miller DH, Thompson AJ, Ciccarelli O. Exploring the relationship between white matter and gray matter damage in early primary progressive multiple sclerosis: An in vivo study with TBSS and VBM. Human Brain Mapping. 2009;**30**:2852-2861

[16] Kolasa M, Hakulinen U, Helminen M, Hagman S, Raunio M, Rossi M, et al. Longitudinal assessment of clinically

isolated syndrome with diffusion tensor imaging and volumetric MRI. Clinical Imaging. 2015;**39**:207-212

[17] Rocca MA, Preziosa P, Mesaros S, Pagani E, Dackovic J, Stosic-Opincal T, et al. Clinically isolated syndrome suggestive of multiple sclerosis: Dynamic patterns of gray and white matter changes—A 2-year MR imaging study. Radiology. 2016;**278**:841-853

[18] Forn C, Barros-Loscertales A, Escudero J, Benlloch V, Campos S, Antonia Parcet M, et al. Compensatory activations in patients with multiple sclerosis during preserved performance on the auditory N-back task. Human Brain Mapping. 2007;**28**:424-430

[19] Lowe MJ, Beall EB, Sakaie KE, Koenig KA, Stone L, Marrie RA, et al. Resting state sensorimotor functional connectivity in multiple sclerosis inversely correlates with transcallosal motor pathway transverse diffusivity. Human Brain Mapping. 2008;**29**:818-827

[20] Lisak RP. Neurodegeneration in multiple sclerosis: Defining the problem. Neurology. 2007;**68**:S5-S12, discussion S43-54

[21] Yount R, Raschke KA, Biru M, et al. Traumatic brain injury and atrophy of the cingulate gyrus. The Journal of Neuropsychiatry and Clinical Neurosciences. 2002;**14**(4):416-423

[22] Hudak A, Warner M, Marquez de la Plata C, Moore C, Harper C, Diaz-Arrastia R. Brain morphometry changes and depressive symptoms after traumatic brain injury. Psychiatry Research. 2011;**191**(3):160-165

[23] Zhou Y. Neuroimaging in Mild Traumatic Brain Injury. New York, USA: Nova Publishers; 2017

[24] Bender AR, Raz N. Normal-appearing cerebral white matter in healthy adults: Mean change over 2 years and individual differences in change. Neurobiology of Aging. 2015;**36**:1834-1848

[25] McCarrey AC, An Y, Kitner-Triolo MH,Ferrucci L, Resnick SM. Gender differences in cognitive trajectories in clinically normal older adults. Psychology and Aging. 2016;**31**:166-175

[26] Zhou Y, Milham MP, Lui YW, Miles L, Reaume J, Sodickson DK, et al. Default-mode network disruption in mild traumatic brain injury. Radiology. 2002;**265**:882-892

[27] Andrews-Hanna JR, Reidler JS, Sepulcre J, Poulin R, Buckner RL. Functional-anatomic fractionation of the brain's default network. Neuron. 2010;**65**:550-562

[28] Zhou Y, Lui YW, Zuo XN, Milham MP, Reaume J, Grossman RI, et al. Characterization of thalamo-cortical association using amplitude and connectivity of functional MRI in mild traumatic brain injury. Journal of Magnetic Resonance Imaging. 2014;**39**:1558-1568

[29] Zhou Y. Abnormal structural and functional hypothalamic connectivity in mild traumatic brain injury. Journal of Magnetic Resonance Imaging. 2017;**45**:1105-1112

[30] Fox MD, Raichle ME. Spontaneous fluctuations in brain activity observed with functional magnetic resonance imaging. Nature Reviews. Neuroscience. 2007;**8**:700-711

[31] Goh JO, An Y, Resnick SM. Differential trajectories of age-related changes in components of executive and memory processes. Psychology and Aging. 2012;**27**:707-719

[32] Zhou Y. Functional Neuroimaging Methods and Frontiers. New York, USA: Nova Publishers; 2018

[33] Bartzokis G. Age-related myelin breakdown: A developmental model of cognitive decline and Alzheimer's disease. Neurobiology of Aging. 2004;**25**:5-18. author reply 49-62

[34] Kodiweera C, Alexander AL, Harezlak J, McAllister TW, Wu YC. Age effects and gender differences in human brain white matter of young to middle-aged adults: A DTI, NODDI, and q-space study. NeuroImage. 2016;**128**:180-192

[35] Scheinost D, Finn ES, Tokoglu F, et al. Gender differences in normal age trajectories of functional brain networks. Human Brain Mapping. 2015;**36**:1524-1535

[36] Trachtenberg AJ, Filippini N, Ebmeier KP, Smith SM, Karpe F, Mackay CE. The effects of APOE on the functional architecture of the resting brain. NeuroImage. 2012;**59**:565-572

[37] Shu H et al. Opposite neural trajectories of apolipoprotein E 4 and 2 alleles with aging associated with different risks of Alzheimer's disease. Cerebral Cortex. 2016;**26**:1421-1429

[38] Kennedy KM et al. Effects of beta-amyloid accumulation on neural function during encoding across the adult lifespan. NeuroImage. 2012;**62**:1-8. DOI: 10.1016/j.neuroimage

[39] Buckner RL. Memory and executive function in aging and AD: Multiple factors that cause decline and reserve factors that compensate. Neuron. 2004;**44**:195-208

[40] Sala-Llonch R, Bartres-Faz D, Junque C. Reorganization of brain networks in aging: A review of functional connectivity studies. Frontiers in Psychology. 2015;**6**:663

[41] Legon W, Punzell S, Dowlati E, Adams SE, Stiles AB, Moran RJ. Altered prefrontal excitation/inhibition balance and prefrontal output: Markers of aging in human memory networks. Cerebral Cortex. 2016;**26**(11):4315-4326

[42] Raichle ME, Mac Leod AM, Snyder AZ, Powers WJ, Gusnard DA, Shulman GL. A default mode of brain function. Proceedings of the National Academy of Sciences of the United States of America. 2001;**98**:676-682

[43] Buckner RL, Snyder AZ, Shannon BJ, LaRossa G, Sachs R, Fotenos AF, et al. Molecular, structural, and functional characterization of Alzheimer's disease: Evidence for a relationship between default activity, amyloid, and memory. The Journal of Neuroscience. 2005;**25**:7709-7717

[44] Jones DT et al. Age-related changes in the default mode network are more advanced in Alzheimer disease. Neurology. 2011;**77**:1524-1531. DOI: 10.1212/WNL.0b013e318233b33d

[45] Fjell AM, Sneve MH, Storsve AB, Grydeland H, Yendiki A, Walhovd KB. Brain events underlying episodic memory changes in aging: A longitudinal investigation of structural and functional connectivity. Cerebral Cortex. 2016;**26**:1272-1286

[46] Kennedy KM, Rodrigue KM, Bischof GN, Hebrank AC, Reuter-Lorenz PA, Park DC. Age trajectories of functional activation under conditions of low and high processing demands: An adult lifespan fMRI study of the aging brain. NeuroImage. 2015;**104**:21-34

[47] Westlye LT, Reinvang I, Rootwelt H, Espeseth T. Effects of APOE on brain white matter microstructure in healthy adults. Neurology. 2012;**79**:1961-1969

[48] Ward AM, Mormino EC, Huijbers W, Schultz AP, Hedden T, Sperling RA. Relationships between default-mode network connectivity, medial temporal lobe structure, and age-related memory

deficits. Neurobiology of Aging. 2015;**36**:265-272

[49] Zhou J, Greicius MD, Gennatas ED, et al. Divergent network connectivity changes in behavioural variant frontotemporal dementia and Alzheimer's disease. Brain: A Journal of Neurology. 2010;**133**:1352-1367

[50] Bilgel M, An Y, Zhou Y, et al. Individual estimates of age at detectable amyloid onset for risk factor assessment. Alzheimer's & Dementia: The Journal of the Alzheimer's Association. 2015;**36**(8):2333

[51] Scholl M, Lockhart SN, Schonhaut DR, et al. PET imaging of tau deposition in the aging human brain. Neuron. 2016;**89**(5):971-982

[52] Sheline YI, Raichle ME, Snyder AZ, et al. Amyloid plaques disrupt resting state default mode network connectivity in cognitively normal elderly. Biological Psychiatry. 2010;**67**:584-587

[53] Tsvetanov KA, Henson RN, Tyler LK, Razi A, Geerligs L, Ham TE, et al. Extrinsic and intrinsic brain network connectivity maintains cognition across the lifespan despite accelerated decay of regional brain activation. The Journal of Neuroscience. 2016;**36**:3115-3126

[54] Worthy DA, Davis T, Gorlick MA, Cooper JA, Bakkour A, Mumford JA, et al. Neural correlates of state-based decision-making in younger and older adults. NeuroImage. 2015;**130**:13-23